Structural, magnetic, and transport properties of nanoparticles of the manganite $Pr_{0.5}Ca_{0.5}MnO_3$

Tapati Sarkar,[a)] P. K. Mukhopadhyay, and A. K. Raychaudhuri
DST Unit for NanoSciences, S.N.Bose National Centre for Basic Sciences, Block JD, Sector III, Salt Lake, Kolkata 700 098, India

Sangam Banerjee
Surface Physics Division, Material Physics Group, Saha Institute of Nuclear Physics, 1/AF, Bidhannagar, Kolkata 700 064, India

In this paper we report the structural, magnetic, and transport properties of nanoparticles of $Pr_{0.5}Ca_{0.5}MnO_3$(PCMO). On comparing our results with that of bulk PCMO, we find that there is a likely destabilization of charge ordering in nanoparticles of PCMO. The investigation has been done with particle sizes as small as 15 nm synthesized by polyol route. The size reduction (by keeping the chemical composition unchanged) reduces the orthorhombic *c* axis preferentially and thus reduces the orthorhombic distortion. The size reduction to 15 nm enhances the ferromagnetic moment at low temperatures and strongly suppresses the activated charge transport which is seen in the bulk samples of charge ordered PCMO.

I. INTRODUCTION

In recent years studies of hole doped perovskite manganites have attracted much attention. The doped perovskite oxide manganites are fascinating because they can readily be tuned between radically different phases by controlling the carrier concentration. In addition, a number of externally controllable parameters can control charge transport in these materials. This makes them attractive as sensor material. Broadly speaking, in these materials we can have either a ferromagnetic metal, a charge-ordered (CO) insulator, or a paramagnetic polaron liquid.[1] The charge ordered state is associated with a real space ordering of 1:1 Mn^{3+}/Mn^{4+} species accompanying a lattice structural change.[2,3] It occurs in many half-doped manganites ($La_{0.5}Ca_{0.5}MnO_3$,[4] $Pr_{0.5}Ca_{0.5}MnO_3$,[5] $Pr_{0.5}Sr_{0.5}MnO_3$,[6] $Nd_{0.5}Ca_{0.5}MnO_3$,[7] $Nd_{0.5}Sr_{0.5}MnO_3$,[8] etc.). The specific case of $Pr_{0.5}Ca_{0.5}MnO_3$ (PCMO), which we have investigated in this paper, has a CO transition around 245 K.[9] The charge ordered phase in $Pr_{1-x}Ca_xMnO_3$ ($0.3 \leqslant x \leqslant 0.5$) has been found to be particularly robust.[10] In $Pr_{0.5}Ca_{0.5}MnO_3$ a high magnetic field of more than 20 T is needed to destabilize ("melt") the CO state. The manganites contain interactions of different types that are often of comparable strengths. As a result, the ground state of the manganites can be of different types depending on which of the interactions win over. In this particular investigation we would like to see what happens to the physical properties of the charge ordered manganites when their particle size is severely reduced. In particular, tuning of the interactions by size offers an interesting possibility to change the resulting ground state and the physical properties of the manganites without changing the chemical composition.

It has been demonstrated by us before that the ferromagnetic transition in $La_{0.67}Ca_{0.33}MnO_3$ can be enhanced by size reduction presumably due to the more cubic nature of the nanoparticles.[11] There have also been reports of greater ferromagnetic interaction in other charge ordered systems such as $Nd_{0.5}Ca_{0.5}MnO_3$ and $Nd_{0.5}Sr_{0.5}MnO_3$ when the grain size is reduced.[12] However, these studies have not investigated the effect of size reduction on the transport properties, and the structural changes have not been investigated to establish whether the change in physical properties on size reduction can be linked to any change in the structural parameters. It will be of interest to investigate whether the enhanced ferromagnetic interaction seen on size reduction can destabilize the charge ordering in the manganites. To be specific, in this work we have investigated what happens to the physical properties of $Pr_{0.5}Ca_{0.5}MnO_3$ (a strongly charge ordered system) when we bring down their sizes from "bulk" (size $\geqslant 3\ \mu m$) to sizes as small as 15 nm. We, in particular, want to investigate what happens to the transport properties of a CO manganite when the size is reduced. We find that there is a clear change of the physical properties which one can relate to the weakening of charge ordering when the size is reduced to the range of a few tens of nanometers. The size reduction leads to the appearance of enhanced ferromagnetic moments. This is accompanied by a change in the transport property such as reduced activation energy for transport and a likely appearance of a "metallic" conduction of percolative nature in the nanoparticles. The magnetic as well as transport data suggest that the size reduction may have weakened the robust charge ordering in PCMO. The size reduction also has a clear effect on the structural parameters which show up in the reduction of the cell volume. The investigation described in detail in subsequent sections presents the synthesis, structural characterization, magnetic, and transport measurements.

[a)]Electronic mail: tapatis@bose.res.in

II. EXPERIMENT

We have adopted the sol-gel based polymeric precursor (polyol) route to synthesize PCMO nanoparticles with sizes down to 10 nm. This method allows synthesis at a significantly lower sintering temperature compared to the conventional solid state procedure. In this technique the polymer (ethylene glycol in our case) helps in forming a close network of cations from the precursor solution and assists the reaction, enabling phase formation at relatively low temperatures.[13] A major challenge encountered in the synthesis of nanocrystalline multicomponent oxides is the poor control of stoichiometry at the nano level. However, our synthesis route ensures homogeneity, phase purity, and a good control over stoichiometry, as brought out by x-ray diffraction (XRD) and chemical tests.

In a typical synthesis process, high purity ($>99\%$) $(CH_3COO)_3Pr \cdot 3H_2O$, $Ca(CH_3CO_2)_2 \cdot H_2O$, and $(CH_3COO)_2Mn \cdot 4H_2O$ (procured from Sigma-Aldrich[14]) were dissolved in the desired stoichiometric proportions in acetic acid and H_2O. To this solution an appropriate amount of ethylene glycol (molecular weight=62.07 gm/mol) was added and heated until the sol was formed. The gel was dried overnight at $\sim 150\ ^\circ C$. Pyrolysis was done at 350 and 450 °C followed by a sintering at $\sim 650\ ^\circ C$ to obtain the desired chemical phase. The process was followed by thermal analysis. The water-ethylene glycol ratio, heat treatment employed during gelling, pyrolization, and calcination were found to influence the particle size of the final product. We optimized these process parameters to obtain phase pure $Pr_{0.5}Ca_{0.5}MnO_3$ particles with size ~ 10 nm (as established from XRD results, using the Williamson-Hall plot[15]).

We used pellets of the nanopowders both for transport and magnetic measurements. The pellets were sintered at different temperatures varying from 370 to 1300 °C and for varying time periods (5–30 h) in an effort to prepare a batch of PCMO samples of varying particle sizes. All the synthesized samples were characterized using powder XRD using Cu $K\alpha$ radiation at room temperature. Additionally, the higher particle size samples (>100 nm) were characterized by field emission gun–scanning electron microscopy (FEG-SEM) to confirm the particle size obtained from XRD. This was done because the accuracy of particle size determination through XRD decreases for higher particle sizes when the broadening due to size becomes less than the instrumental broadening. In the same run we also checked by energy dispersive x-ray analysis (EDAX) the variation in relative Pr:Ca:Mn concentration as a function of position (with length resolutions of ~ 100 nm) over length scales of $\sim 1\ \mu m$. The pellets were also checked for oxygen stoichiometry using iodometric titration. The magnetic characterizations have been carried out using a quantum design superconducting quantum interference device (SQUID) magnetometer.[16] The resistivity measurements were done using standard dc four-probe technique in the temperature range of 4.2–300 K in a closed cycle refrigerator.[17] The magnetoresistance (MR) measurements up to $H=10$ T have been carried out in bath-type cryostat.

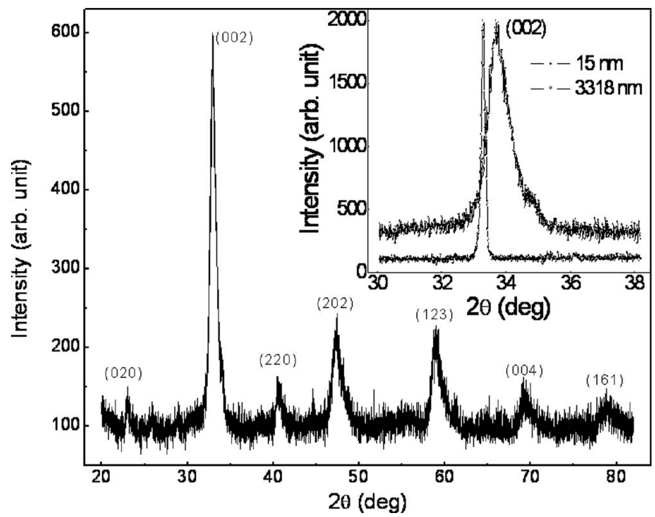

FIG. 1. (Color online) XRD pattern of PCMO nanocrystals.

III. RESULTS

A. Structure

Figure 1 shows the XRD pattern of PCMO nanoparticles. Similar XRD patterns were taken for all the PCMO samples (pellets). The average particle size of the unpelletized synthesized particles as calculated from XRD data came out to be around 10 nm. Starting from nanoparticles of average size of 10 nm, the smallest particle size that we get after pelletization and heat treatment is 15 nm. We synthesized six different size samples having particle sizes ranging from 15 to 3.3 μm by varying the annealing time and temperature as stated above. Figure 2 gives a plot of the variation of the average particle size with the annealing temperature. The preparation technique of the sample thus allows us to control the average size from down to 15 nm up to nearly 3.3 μm. The size distributions as established from transmission electron microscopy (TEM) (for smaller particles) and SEM (for larger particles) show that, for the nanoparticles, typically the width of distribution is $\approx \pm 15\%$. For the larger particles

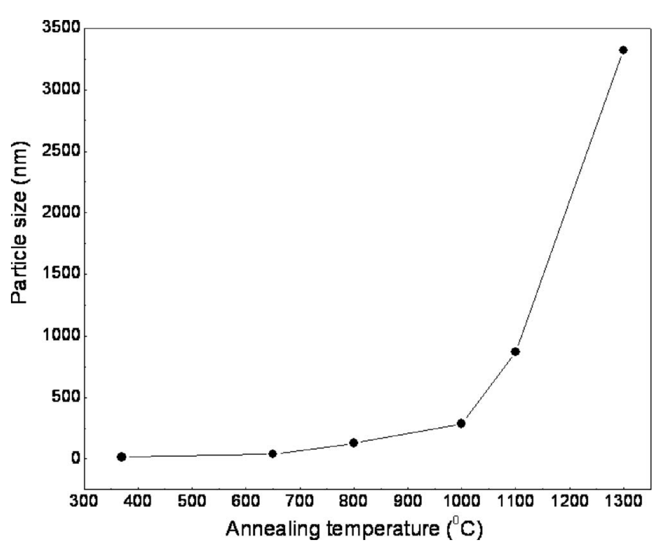

FIG. 2. (Color online) Variation of average particle size with the annealing temperature.

TABLE I. Annealing conditions [temperature (T), time (t), particle size (d), lattice parameters (a, b, and c) (typical error is ±0.001 Å), cell volume (CV) (typical error is ±0.1 Å^3), and asymmetry parameter (δ) (typical error is ±0.0002)] of PCMO pellets.

T (°C)	t (h)	d (nm)	a (Å)	b (Å)	c (Å)	CV (Å^3)	δ
370	5	15	5.334	5.318	7.526	213.5	0.4131
650	10	38	5.344	5.332	7.549	215.1	0.4142
800	10	128	5.368	5.339	7.578	217.2	0.4155
1000	10	287	5.387	5.364	7.631	220.5	0.4196
1100	30	870	5.398	5.365	7.668	222.1	0.4249
1300	2	3318	5.398	5.365	7.671	222.2	0.4254

(size > 1 μm), the size distribution is broader (±20%) because the particles were made to grow thermally. For the "bulk" sample with average particle size of 3.3 μm, 80% of the particles have size in excess of 2 μm. The XRD data were used to estimate the average particle size (see Table I). With a decrease in particle size, a shift of the XRD peaks was observed towards higher angle implying smaller lattice spacing. The inset in Fig. 1 shows the (002) peak for the samples with lowest and highest particle sizes. A clear shift of the 2θ value towards higher angle is observed for the nanosample.

The diffraction data of the pellets were also analyzed using the Rietveld powder diffraction profile fitting technique to obtain the crystal structure parameters. The data was fitted to the orthorhombic space group *Pnma*.[18] Our x-ray profiles were modeled using a pseudo-Voigt profile shape function. For the smallest particles, the cell volume is 213.52 Å^3. This is smaller by 3.9% than the cell volume of 222.18 Å^3 estimated for the bulk sample. The cell volume of our bulk sample matches with the reported standard value[18] of 221.92 Å^3. (By bulk sample we imply particles with size in excess of 1 μm.) The size reduction also decreases the orthorhombic distortion which is measured by the parameter $\delta=[\sqrt{2}c/(a^2+b^2)^{1/2}]-1$. For a cubic structure $\delta=0$. The variations of cell volume and δ with the particle size are shown in Fig. 3. In the same graph we also show the change (% decrease) of the cell parameters a, b, and c as a function of size. (Note, the x axis is plotted as 1/size to accentuate the lower size region.) As the particle size decreases, the cell volume and the asymmetry parameter initially decrease rather quickly to a size of ~150 nm, and after that the decrease is more gradual. The structural parameters as calculated from the XRD data for all the samples are shown in Table I. For investigation of the physical properties we have selected the two end members, namely, a sample with average particle size of 15 nm (referred to as nanosample) and a sample with average particle size of 3 μm (referred to as bulk sample).

We checked the oxygen stoichiometry of the pellets by iodometric titration. All the pellets had some oxygen deficiency ($Pr_{0.5}Ca_{0.5}MnO_{3-\epsilon}$) with ϵ positive. $\epsilon \approx 0.022$ for the pellet with the smallest particle size and it increases somewhat for the bulk sample. Particles with smaller particle size have better oxygen stoichiometry.

B. Magnetization measurements

Figure 4 shows the temperature dependence of magnetization of PCMO for both bulk sample (average particle size ~3.3 μm) and nanosample (average particle size ~15 nm) taken at $H=2$ T. For the bulk sample, the charge ordering transition is clearly seen as a peak at $T=250$ K. This is similar to that reported in PCMO samples with particle size larger than 1 μm prepared by conventional ceramic route.[19,20] In contrast, for the sample with 15 nm particle size, the magnetization rises monotonically as the temperature is lowered with a small shoulder in the vicinity of $T=250$ K. We do not find a peak in the magnetization that is observed in the CO samples. We thus observe that for the nanoparticle the magnetization is distinct from that seen in the bulk sample and there is a large enhancement of the moment at low temperatures. However, we note that while the magnetization M does increase as T is lowered, the M-T curve is not exactly what one would expect for a ferromagnet with a proper long-range order where one sees a sharp transition at the ferromagnetic transition. It is likely that the re-

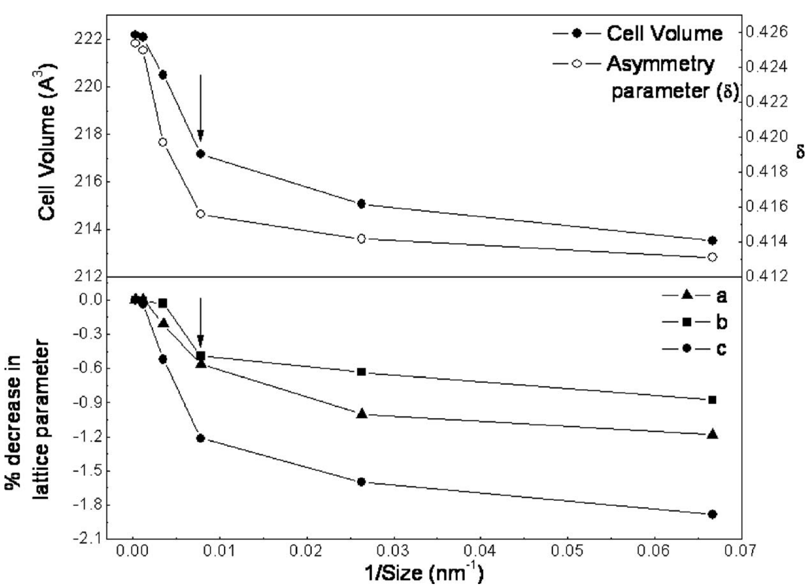

FIG. 3. (Color online) Variation of cell volume, asymmetry parameter, and change of cell parameter with particle size.

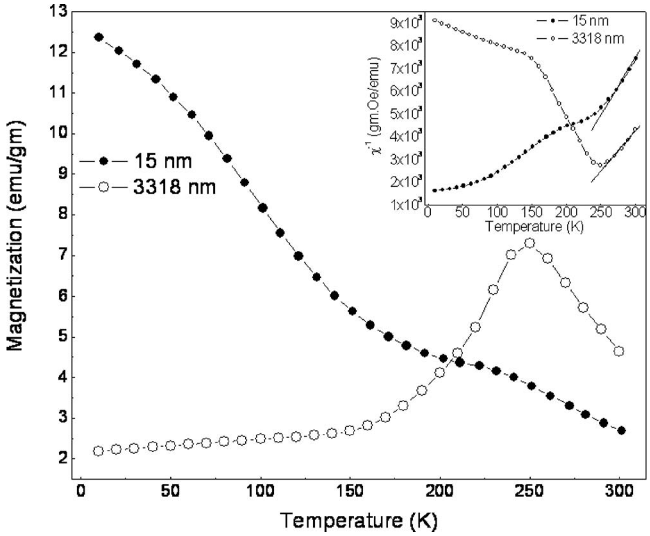

FIG. 4. (Color online) Magnetization vs temperature for bulk and nano-PCMO under a magnetizing field of 2 T.

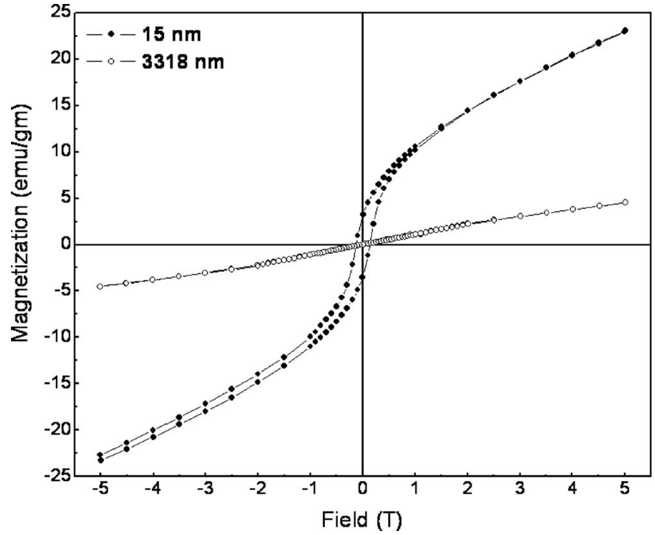

FIG. 5. (Color online) Magnetization vs magnetic field for bulk and nano-PCMO at a temperature of 5 K.

sulting phase in the nanoparticle is a disordered ferromagnet. The shallow shoulder at $T \approx 250$ K suggests that there may be a small fraction of charge ordered particles coexisting with a majority phase that have lost the charge ordering.

In the inset of the figure we have shown a plot of inverse susceptibility $1/\chi$ versus temperature for the two samples. We have taken $\chi = M/H$. In the paramagnetic region the data can be fitted to the Curie-Weiss law $[\chi = C/(T-\theta)]$, where C is the Curie constant and θ is the Weiss temperature. The paramagnetic Curie temperature in both samples is nearly identical and positive. The θ for the bulk sample is ≈ 229 K and that for the nanosample is ≈ 231 K. From the Curie constant C, we calculated the effective magnetic moment μ_{eff}. For the bulk sample $\mu_{\mathrm{eff}} \approx 3.72\mu_B$, and for the nanosample $\mu_{\mathrm{eff}} \approx 3.51\mu_B$. This is comparable to the μ_{eff} in most manganites. This establishes that the paramagnetic state of PCMO is not much affected by the particle size. The main effect arises below the CO transition and the magnetic order (or its absence) at low temperatures distinguishes them. This is indeed interesting since the two samples are chemically identical and have nearly identical paramagnetic state, but the bulk sample becomes charge ordered while the nanosample has larger moment and leads to a disordered ferromagnet.

While there is an enhancement of the magnetic moment in the nanoparticles as revealed through the magnetization, it is apparent that there is an absence of a proper long-range ferromagnetic (FM) order. The absence of a long range FM order can also be seen in the hysteresis curve shown in Fig. 5. The MH loops (at 5 K) for the bulk and nanosamples are shown. The magnetic field is varied from -5 to $+5$ T. The nanoparticle shows a small hysteresis loop which closes at ~ 1 T. (There is a small shift in the fourth quadrant of the MH loop which arises due to thermal drift. The shift in the magnetization value is only $\sim 2.7\%$, which is quite small.) There is a small coercive field $(H_c) \approx 0.1$ T. However, the magnetization does not saturate even at a field of 5 T which is another signature of disorder in the resulting ferromagnetic state. The bulk sample, in contrast, does not show any such hysteresis loop. It has a small moment of $0.16\mu_B$/f.u. even at 5 T. For the nanoparticle the observed moment (at 5 T) is much larger $= 0.80\mu_B$/f.u. However, this is smaller than the moment ($\approx 3.5\mu_B$/f.u.) seen in ferromagnetic manganites such as $La_{0.7}Ca_{0.3}MnO_3$. The reduction in moment is likely due to large contribution of disordered spins in the surface as well as in the grain boundaries that constitute a good fraction of the nanosample. To summarize, we find that there is a rather strong enhancement of the ferromagnetic moments in the nanoparticles that are not charge ordered but the resulting state, though FM has substantial disorder that presumably prevents formation of long-range FM order.

C. Electrical transport

The electrical resistivities in the manganite samples have been studied from 4.2 to 300 K. In Fig. 6 we show the behavior of the resistivity of two samples (the samples with largest and smallest particle sizes) as a function of tempera-

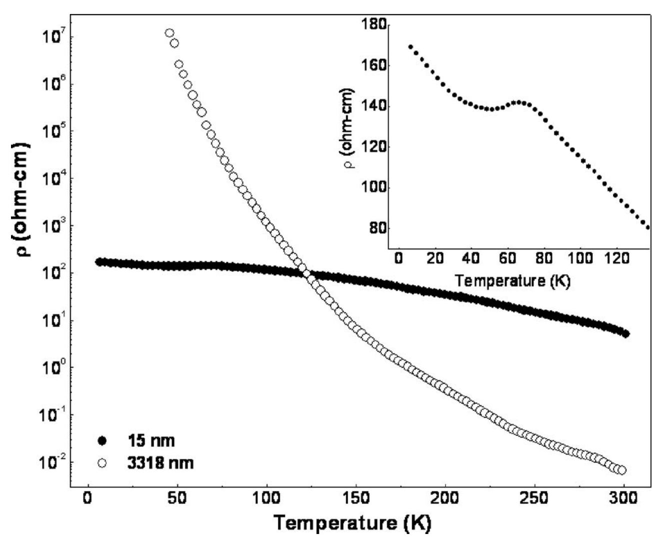

FIG. 6. (Color online) Resistivity vs temperature curves for PCMO pellets with two different particle sizes. Inset shows the resistivity vs temperature curve for the nanoparticle sample in the low temperature region.

ture. With the particle size being small, the transport experiments suffer from the presence of a large contribution of grain boundaries in the electrical transport. However, in spite of the presence of the contribution of grain boundaries, one can find distinct effects of size reduction which are not arising from the grain boundary contribution alone. In nanoparticles the resistivity at room temperature is about three orders higher than that of the bulk sample. This is not unexpected because, though the two materials are expected to have similar properties in the paramagnetic state at high temperature, with the surface-to-volume ratio in the nanosample being 200 times larger, the grain boundary contribution to the resistivity is larger leading to larger resistivity. In the bulk sample, however, the resistivity rises rapidly as the sample is cooled through the CO transition at $T \approx 250$ K. The bulk sample reaches the ρ of the nanosample at $T \approx 120$ K but at $T \approx 50$ K it reaches a value which is nearly five orders more than the nanosample. [Here it may be noted that bulk $Pr_{0.5}Ca_{0.5}MnO_3$ shows no insulator-metal transition. This is in contrast to bulk $Nd_{0.5}Ca_{0.5}MnO_3$, which does show an insulator-metal transition in zero field. This difference in behavior can be traced to the fact that the ground state in manganites depends on the relative contribution of the double exchange mechanism (which favors ferromagnetism along with metallic conductivity) and the superexchange interaction between the manganese ions (which favors antiferromagnetic order and insulating electric properties). In $Nd_{0.5}Ca_{0.5}MnO_3$, the peak in resistivity (or the insulator-metal transition) is related to the magnetic state of the material. Upon cooling, the magnetization of $Nd_{0.5}Ca_{0.5}MnO_3$ increases, and this increase in magnetization is associated with a corresponding decrease in resistivity. In $Pr_{0.5}Ca_{0.5}MnO_3$, the bulk sample shows no increase in magnetization (Fig. 4), and as such no decrease in resistivity, i.e., no insulator-metal transition.] For the sample with nanoparticles, the resistivity also rises upon cooling, but the rise is much less rapid and at low temperature the resistivity change actually reverses trend with a shallow maxima and minima (see inset of Fig. 6). Thus the resistivity data show that there is indeed a difference between the bulk sample and the sample with nanoparticles. The activated transport with a steep activation energy in the CO bulk sample is strongly suppressed in the nanosample. The charge ordering transition is reflected in the transport property as a change in slope in the resistivity plot at ~250 K in the bulk sample. To highlight this, we show in Fig. 7 the derivative $d \ln \rho / d(1/T)$ which gives the transport activation energy at temperature T. For the bulk sample we find a clear change in slope at the CO temperature of $T = 250$ K showing hardening of the transport gap on cooling through the CO temperature. The bulk sample thus shows an insulating behavior throughout the temperature range and the continuous increase in the activation energy on cooling can be seen through enhancement of $d \ln \rho / d(1/T)$ on cooling. The observed data are consistent with the expectation from a charge ordered system. The nanosample with 15 nm particle size has a resistivity that increases as T is lowered but unlike the bulk sample there is no clear change in slope at around 250 K which one would expect if the system shows a CO transition. If anything, it shows a gradual decrease in slope

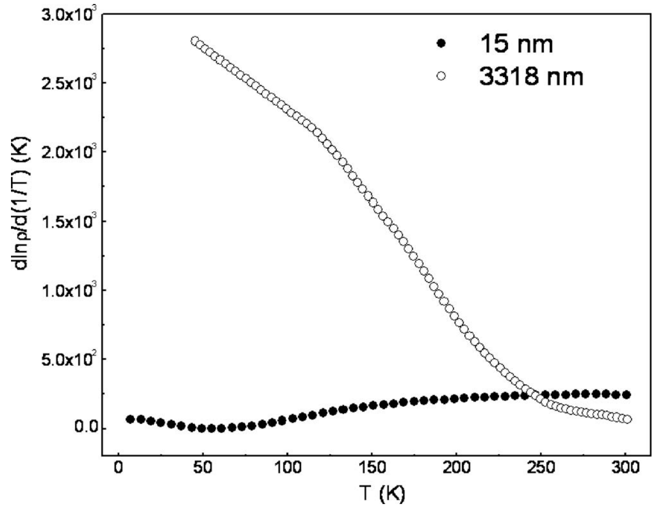

FIG. 7. (Color online) Derivative $d \ln \rho / d(1/T)$ as a function of T for the bulk and nanoparticle samples.

as can be seen in the variation of $d \ln \rho / d(1/T)$ as a function of T shown in Fig. 7. It is interesting to note that in the nanosample there is a shallow hump in the resistivity at ~65 K beyond which ρ decreases on cooling although not very drastically. This is shown as an inset in Fig. 6. The resistance shows a shallow minima and again starts rising from 50 K. This decrease in resistance from 65 to 50 K is a signature that the sample with nanoparticles may have a small metallic fraction which is coexisting with a dominating insulating phase. The metallic fraction is far below the percolation threshold and there is also a large contribution of activated transport through the grain boundaries as a result of which the sample never shows a clear metallic behavior. The absence of a clear CO transition in the resistivity of the nanosample, a possible appearance of a small metallic phase at low temperatures, and appearance of a strong ferromagnetic magnetic moment in the nanosample thus appear to be correlated, and they suggest that the CO state seen in the bulk is weakened (or destabilized) by size reduction.

The MR of the nanosample also shows a change in the dominant characteristics. In bulk sample of PCMO ($x = 0.5$) the CO state is very rugged and fields larger than 20 T are needed to melt the charge order and obtain the metallic phase.[21] In contrast, the nanosample shows a finite MR even at a field of $H = 10$ T. The MR measurements were done for the nanosample (average size of 15 nm) from 4.2 to 300 K and under a field of 10 T. The MR ($\mathrm{MR} = 100[\rho(H) - \rho(0)]/\rho(0)$) values are shown in Fig. 8. The MR is negative. It is seen that down to ~70 K, the magnetic field has very little effect on the resistance and the MR is very low even in a field of 10 T. However, below 70 K, the field starts showing its effect, and there is a sharp rise in magnetoresistance. At the lowest temperature, the magnetoresistance reaches a value of ~−38%. We may note that the temperature at which the MR appears (rather suddenly) is the temperature (65 K) at which there is a small peak in ρ and ρ decreases on cooling. We can interpret the MR in the nanosample as a signature of weakening or destabilization of the CO that pulls down the magnetic field at which the CO can be made to "melt."

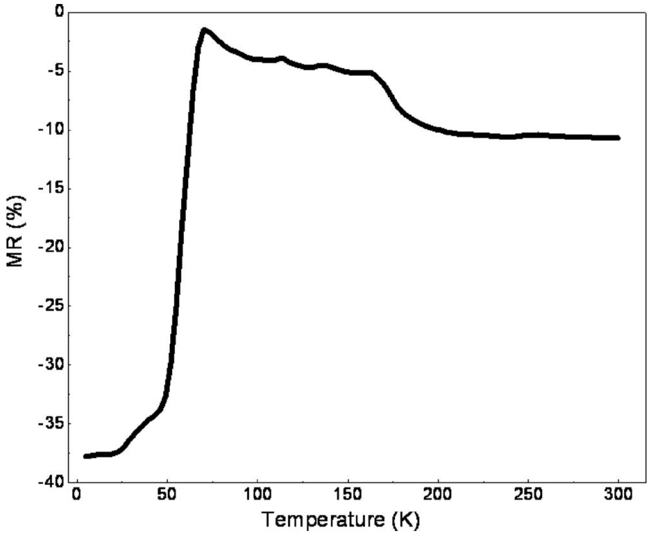

FIG. 8. (Color online) Negative MR curve for PCMO pellet (particle size ~15 nm).

IV. DISCUSSIONS

The data presented above show very clearly that the structural, magnetic, and electronic transport properties of the sample with nanoparticles is distinctly different from those of the bulk. The nanosample has a more compact unit cell and lower asymmetry parameter, higher magnetic moment with no signature of a CO transition in the magnetic susceptibility, absence of a definitive signature of a CO transition in the resistivity, and appearance of a small metallic phase and a substantial MR even in a field of 10 T. We would like to suggest that the results presented above can be taken as the signature of a much weakened charge ordering in the nanosized sample. The charge ordering seen in bulk sample of PCMO can thus be partly destabilized in nanoparticles. The resulting phase has strong ferromagnetic moments and some fraction of metallic phase although it is not a good metal with a long range FM order.

The size reduction has a distinct signature in the crystal structure. There is a compaction of the unit cell as the size is reduced. The reduction in the cell volume of the PCMO nanoparticles can arise due to an increased surface pressure in the nanoparticles. Assuming the particles to be spherical in shape, it is known that there is a surface pressure $P=2S/d$, where d is the diameter of the particle and S is the surface tension. This higher pressure can lead to a reduction of the cell volume from 222.2 to 213.5 Å^3 as in our case. Using a bulk modulus $B\approx150$ GPa, a typical figure for many oxides,[22] we find that a pressure of ≈ 6 GPa is needed to produce the change of cell volume as observed in the experiment. Such a pressure can be produced if the surface tension $S\approx 90$ N/m.

It is also established that the size reduction leads to significant changes in lattice parameters. It appears, if one follows the structural evolution on size reduction, that the destabilization of the charge ordering in the nanoparticles is associated with a small but clear reduction in the orthorhombic distortion. It is likely that the reduction of such a distortion leads to the enhancement of Mn–O–Mn bond angle closer to 180 °C and the reduction in cell size will lead to compaction of the Mn–O bond lengths. These two factors will make the bandwidth increase which will lead to strengthening of the ferromagnetic interaction. The enhancement of the ferromagnetic interaction (and the resulting kinetic energy gained by the electron) will make any insulating state unstable and this would lead to destabilization of the charge ordering.

It is also to be noted that there are a large number of spins on the surface of nanoparticles that are generally expected to be disordered and will lead to destruction of any spin order. Absence of any long-range FM order is likely to be the manifestation of a large number of disordered spins on surfaces of nanoparticles. It may also be possible that these large numbers of surface atoms will also weaken the cooperative orbital order that is needed to stabilize the insulating state of the charge ordered phase.

In ABO_3 perovskite oxides it is established that the size reduction leads to changes in structural symmetry.[23] This in turn can lead to changes in physical properties. The collapse of ferroelectric transition in lead zirconia titanate (PZT) is an example. The size tuning of the ground state properties of manganite nanoparticle is another such example. Manganites have competing interactions with almost equal strengths. The size tuning thus provides a subtle change in balance of relative strengths leading to destabilization of one phase.

V. CONCLUSIONS

In summary, we have studied the effect of size reduction on charge ordering in $Pr_{0.5}Ca_{0.5}MnO_3$ nanoparticles which were successfully synthesized using the polymeric precursor route. All the samples were single phase (chemically). Using our particular synthesis process, we could obtain the perovskite phase formation at a much lower temperature (~650 °C) compared to the standard solid state synthesis route. It has been established that the size reduction (from ~ few micrometers to ~15 nm) substantially weakens or destabilizes the charge ordered state leading to phases with enhanced ferromagnetic moment and traces of metallic conduction. The size reduction also reduces the magnetic field that is needed to melt the charge ordering.

ACKNOWLEDGMENTS

The MR measurements were done at the DST Facility for Low Temperature and High Magnetic Field at IISc, Bangalore, India. The authors would like to thank the Department of Science and Technology, Government of India for financial support. One of the authors (T.S.) also thanks UGC, Government of India for fellowship.

[1] *Collosal Magnetoresistance, Charge Ordering and Related Properties of Manganese Oxides*, edited by C. N. R. Rao and B. Raveau (World Scientific, Singapore, 1998).
[2] C. N. R. Rao, A. Arulraj, A. K. Cheetham, and B. Raveau, J. Phys.: Condens. Matter **12**, R83 (2000).
[3] C. N. R. Rao, A. Arulraj, P. N. Santosh, and A. K. Cheetham, Chem. Mater. **10**, 2714 (1998).
[4] P. G. Radaelli, D. E. Cox, M. Marezio, and S. W. Cheong, Phys. Rev. B **55**, 3015 (1999).
[5] S. Mori, T. Katsufuji, N. Yamamoto, C. H. Chen, and S. W. Cheong, Phys.

Rev. B **59**, 13573 (1999).
[6]R. Kajimoto, H. Yoshizawa, Y. Tomioka, and Y. Tokura, Phys. Rev. B **66**, 180402 (2002).
[7]T. Vogt, A. K. Cheetham, R. Mahendiran, A. K. Raychaudhuri, R. Mahesh, and C. N. R. Rao, Phys. Rev. B **54**, 15303 (1996).
[8]H. Kawano, R. Kajimoto, H. Yoshizawa, Y. Tomioka, H. Kuwahara, and Y. Tokura, Phys. Rev. Lett. **78**, 4253 (1997).
[9]Y. Tomioka, A. Asamitsu, H. Kuwahara, Y. Moritomo, and Y. Tokura, Phys. Rev. B **53**, R1689 (1996).
[10]M. R. Lees, J. Barratt, G. Balakrishnan, D. McK. Paul, and M. Yethiraj, Phys. Rev. B **52**, R14303 (1995).
[11]K. Shantha Shankar, S. Kar, G. N. Subbanna, and A. K. Raychaudhuri, Solid State Commun. **129**, 479 (2004).
[12]L. Sudheendra, H. D. Chinh, A. R. Raju, A. K. Raychaudhuri, and C. N. R. Rao, Solid State Commun. **122**, 53 (2002).
[13]K. Shantha Shankar and A. K. Raychaudhuri, J. Mater. Res. **21**, 27 (2006).
[14]Sigma-Aldrich, Inc., 3050 Spruce Street, St. Louis, MO 63103.
[15]G. K. Williamson and W. H. Hall, Acta Metall. **1**, 22 (1953).
[16]MPMS SQUID Magnetometer, 6325 Lusk Boulevard, San Diego, CA 92121-3733.
[17]Cryomech, Model PT405 Cryogenic Refrigerator, 113 Falso Drive, Syracuse, New York 13211.
[18]P. M. Woodward, T. Vogt, D. E. Cox, A. Arulraj, C. N. R. Rao, P. Karen, and A. K. Cheetham, Chem. Mater. **10**, 3652 (1998).
[19]E. Pollert, S. Krupicka, and E. Kuzmicová, J. Phys. Chem. Solids **43**, 1137 (1982).
[20]Z. Jirák, F. Damay, M. Hervieu, C. Martin, B. Raveau, G. André, and F. Bourée, Phys. Rev. B **61**, 1181 (2000).
[21]M. Tokunaga, N. Miura, Y. Tomioka, and Y. Tokura, Phys. Rev. B **57**, 5259 (1998).
[22]A. Bid, A. Guha, and A. K. Raychaudhuri, Phys. Rev. B **67**, 174415 (2003).
[23]S. Chattopadhyay, P. Ayyub, V. R. Palken, A. V. Gurjar, R. M. Wankar, and M. Multani, J. Phys.: Condens. Matter **9**, 8135 (1997).